HiSST: 2nd International Conference on
High-Speed Vehicle Science Technology
11–15 September 2022, Bruges, Belgium

Concept 4: A Reusable Heavy-Lift Winged Launch Vehicle using the In-Air-Capturing Method

Sven Stappert[1], Martin Sippel[1], Steffen Callsen[1], Leonid Bussler[1]

Abstract

Reusability is expected to significantly lower launch costs if refurbishment and recovery costs can be kept low. To analyze and understand the impact of reusability on launch systems, the DLR is conducting studies of reusable space transportation configurations. In this context, a range of promising semi-reusable launch vehicles with a winged reusable first stage and either one or two expendable upper stages for an injection into a geostationary transfer orbit (GTO) were designed and investigated. Different engine and propellant combinations, using either LOX-LH2 or LOX-LCH4, were studied in order to identify potentials and drawbacks of each combination. The winged first stage is recovered by the "In-Air-Capturing" method which is currently studied in the framework of the Horizon 2020 funded project FALCon. A special focus is put onto the aerodynamic behavior of the winged stages. Since the stage performs a mostly aerodynamically controlled re-entry, transitioning from supersonic velocity of Mach 6-9 down to subsonic velocity, the vehicle has to be controllable throughout a vast range of different aerodynamic states. Therefore, a reference stage from the system analysis is selected and subjected to an investigation of dynamic behavior, controllability and stability along a reference trajectory. The insights from this analysis shall be used to re-evaluate the system design and determine implications on a system level.

Keywords *Reusability, LOX/LH2, LOX/LCH4, Reentry, In-Air-Capturing, Flight Dynamics*

Nomenclature

3STO	Three Stage to Orbit
AoA	Angle of Attack
CoG	Center of Gravity
DOF	Degrees of Freedom
GLOM	Gross Lift-Off Mass
GTO	Geostationary Transfer Orbit
IAC	In-Air-Capturing
LCH4	Liquid Methane
LEO	Low Earth Orbit
LH2	Liquid Hydrogen
LOX	Liquid Oxygen
LQR	Linear Quadratic Regulator
MECO	Main Engine Cut-Off
RCS	Reaction Control System
RLV	Reusable Launch Vehicle
SLME	SpaceLiner Main Engine
SSO	Sun-Synchronous Orbit
TRL	Technology Readiness Level
TSTO	Two Stage to Orbit
UAV	Unmanned Aerial Vehicle
VTHL	Vertical Takeoff, Horizontal Landing
VTVL	Vertical Takeoff, Vertical Landing

[1] *German Aerospace Center - DLR, Institute of Space Systems, Space Launcher Systems Analysis – sven.stappert@dlr.de*

1. Introduction

While reusability in space transportation can have a strong impact on the costs and thus competitiveness of space launchers, the historic Space Shuttle has also shown that this impact does not necessarily have to be favorable if the refurbishment costs cannot be kept low. Nonetheless, the recent successes of SpaceX (with Falcon 9 and Falcon Heavy) and Blue Origin (New Shephard) in landing, recovering and reusing their respective booster stages by means of retro propulsion have shown the possibility of developing, producing and operating reusable launchers at low launch service costs. This has raised the interest in introducing reusability to European launchers as a way to lower the launch costs and stay competitive in the evolving launch market. Additionally, the development of Ariane 6 is almost finished and the maiden flight will take place soon. Due to the recent evolvements on the international launcher market it is of crucial importance to start elaborating on possible Ariane 6 successors.

In the wake of this increased interest in future launch vehicles incorporating reusability, several studies throughout Europe have been initiated. The CNES launch directorate is assessing launch system definitions of for the next generation of Ariane launch vehicles, so called Ariane NEXT [1]. At DLR the projects AKIRA, XTRAS, TRANSIENT and the FALCon project are the most mentionable [2]-[5]. In the two former projects a broad comparison of RLV strategies was the main goal. Here, different return strategies such as vertical landing (VTVL) and horizontal landing (VTHL) were compared to each other. In the FALCon project, the focus is set on studying the In-Air-Capturing (IAC) method for winged, horizontally landing stages and raising the TRL by demonstrating the capturing procedure with subscale UAVs. The In-Air-Capturing recovery method is also used as baseline for the herein shown reusable launchers.

Since this procedure is suitable for winged stages only, a possible RLV configuration which is capable of delivering heavy payloads to orbit (GTO, LEO, SSO) has to be defined which could use this procedure in the future. In this context, 3STO systems were defined that consist of a reusable winged first stage and an expendable second and expendable third stage. The first stage is returning to earth to be captured and recovered via IAC. This heavy-lift system shall be capable of transporting payloads of about 13 -14 tons into GTO. As propellant combinations, LOX-LH2 or LOX-LCH4 are used. For engines using LOX-LH2, a staged combustion version based on the SLME is used [13] as well as a gas generator engine derivative of the Prometheus methalox engine which is currently under development in Europe [14]. For upper stage application, the Vinci engine is used. As LOX-LCH4 engines, the Prometheus methane version is foreseen. In this paper, different launch systems based on a combination of those engines are presented to identify differences between the systems and propellant combinations.

Furthermore, the flight dynamics of a selected winged first stage during re-entry are investigated. Since the re-entering stage covers a vast range of velocities and AoAs, the stage has to be controllable at different flight conditions. It is a challenging task to unite the requirements for supersonic flight with high AoA with the requirement for high Lift-to-Drag ratio required for IAC at subsonic velocity. Thus, it is important to understand the interaction between geometric layout with controllability and its impact onto the stage design.

2. Assumptions & Methods

The launcher is to be designed for the most suitable combination of high commonality in major components and providing good mission flexibility. The upper payload range should be in the order of 12 to 15 tons to GTO and should include multiple payload deployment capability. The vehicles should be capable of performing secondary missions to LEO, MEO or SSO. The expendable section could be single stage or two-stage, hence the launcher results in a 2- or 3-stage to orbit configuration. The TRL of all implemented technologies needs to reach 5 to 6 in 2030 for full-scale development-start enabling operational capability in approximately 2035. The design target for the RLV is 150 missions and between 5 to 10 missions for the engines.

All presented RLV-configurations in this paper are assuming similar key mission requirements:

- GTO: 250 km x 35786 km x 5°
- Argument of Perigee: 0°/180°
- Launch site: CSG, Kourou, French Guiana

The herein presented RLVs are designed as 3STO concepts, with potential service into low-energy target orbits, such as LEO, as TSTO. Past investigations included also TSTO concepts, however, they were deemed unviable due to the comparably high take-off mass [6]. However, low-energy orbits such as LEO or SSO could be served by a 3STO based vehicle using only two stages. Nevertheless, this was not investigated in the framework of this paper.

As for the 3STO launcher architecture the first stage is designed as winged RLV as shown in Fig. 1. The expendable stage/stages are attached in parallel configuration on top of the 1st stage. For 3STO stages the 3rd stage equips the payload. In case of 3STO systems the fairing covers all of the third stage and the payload and hence connects to the upper part of the interstage.

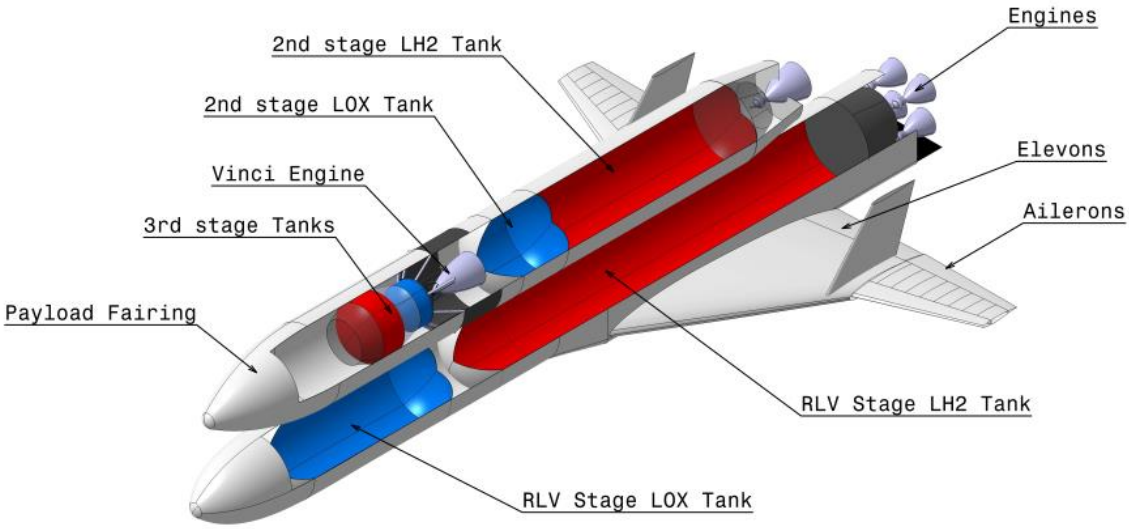

Fig. 1: Exemplary Launcher architecture for a 3STO launcher

The winged first stages are all designed with a double-delta wing and aerodynamic control surfaces at the trailing edges. The inner flaps can be used as elevons while the outer flaps can be used as ailerons for greater control. Furthermore, two vertical rudders are positioned on both wings. The aerodynamic design has to fulfil two major design requirements: first, the stage shall be trimmable and controllable at high AoA during the initial phase of re-entry. Second, the stage has to have a rather high L/D ratio, optimally greater than 6, at subsonic velocity to facilitate the In-Air-Capturing maneuver (see section 2.2 for details).

2.1. Propulsion System

Since different propellant combinations are investigated in this study, a range of various engines is considered as propulsion system for first and upper stages. For first and second stages, the engines are varied depending on propellant combination and required expansion ratio, for third stages the Vinci engine is considered for all options.

As staged combustion LOX-LH2 engine, the SpaceLiner Main Engine (SLME) is selected. This engine has been preliminarily designed and studied at DLR and was originally envisioned for the SpaceLiner passenger transport concept [13]. This engine features moderate 16 MPa of chamber pressure and a Full-Flow Staged Combustion Cycle with a fuel-rich preburner gas turbine driving the LH2-pump and an oxidizer-rich preburner gas turbine driving the LOX-pump [9]. In the context of this work, the RLV first stage is equipped with several SLMEs with an expansion ratio of $\epsilon = 33$ (see Fig. 2). The expendable second stage is equipped with an SLME with a higher expansion ratio of $\epsilon = 59$ to improve performance at lower ambient pressure conditions. The technical data of the SLME, based on cycle analyses from [9] and [13], and Vinci engine are shown in Table 1.

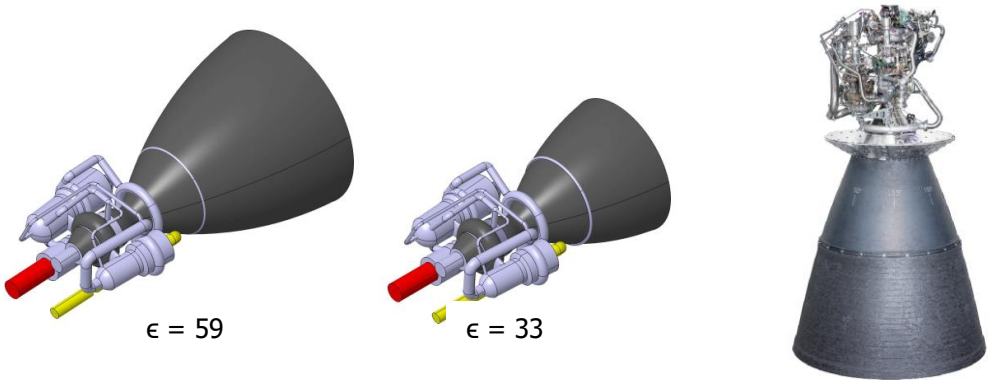

Fig. 2: SLME engine (left) with different expansion ratios and Vinci engine (right)

The SLME engine has a vacuum thrust of up to 2350 kN and sea-level thrust of 2100 kN for the booster engine and 2400 kN, respectively 2000 kN for the second stage. All these values are given at a mixture ratio of 6.5 with a nominal operational MR-range requirement from 6.5 to 5.5. The intended SLME architecture allows to use the booster engines as engines for the ELV stage, after reaching the end of their expected lifetime. The size of the SLME in the small expansion ratio version is a maximum diameter of 1800 mm and overall length of 2981 mm. The larger second stage SLME has a maximum diameter of 2370 mm and overall length of 3893 mm. A size comparison of the two variants and overall arrangement of the engine components is published in [13].

Table 1: Engine Data of SLME and Vinci engines

	RLV Booster	2nd ELV Stage	Vinci
Mixture ratio [-]	6.5	5.5	5.8
Chamber pressure [MPa]	16.9	15.1	6.1
Mass flow per engine [kg/s]	555	481	39
Expansion ratio [-]	33	59	175
Specific impulse in vacuum [s]	435	451	457
Specific impulse at sea level [s]	390	357	-
Thrust in vacuum [kN]	2356	2116	174.8
Thrust at sea level [kN]	2111	1678	-

Table 2: Prometheus and Prometheus-H engine data

	Prometheus RLV Booster	Prometheus 2nd ELV stage	Prometheus -H RLV Booster	Prometheus -H 2nd ELV stage
Mixture ratio [-]	2.68	2.68	6.0	6.0
Chamber pressure [MPa]	12	12	12	12
Mass flow [kg/s]	422.5	422.5	325	325
Expansion ratio [-]	20	59	20	59
Specific impulse in vacuum [s]	319	337	405	431
Specific impulse at sea level [s]	287	251	365	317
Thrust in vacuum [kN]	1322	1397	1292	1375
Thrust at sea level [kN]	1190	1040	1164	1011

In Europe, the current engine development is focused on the Prometheus engine [14]. This gas generator engine is supposed to develop a vacuum thrust of around 1 MN, using LOX-LCH4 as propellant combination. This engine is supposed to be used on the Themis demonstrator and a possible successor of the Ariane 6. Additionally, interest has been expressed in developing a hydrogen-based version of the Prometheus engine, in the following called Prometheus-H. The use of hydrogen would greatly increase the efficiency due to a higher specific impulse, but at the expense of more challenging

propellant and thermal operations. This engine variant would require a dual-shaft turbopump but its overall design can be similar to the baseline Prometheus methane version.

Since the Prometheus engine is currently under development and the publicly available data is limited, the engine model used in this study is based on DLR assessments using a combination of in-house tools and the commercial tool RPA. The data do not necessarily reflect the characteristics of the precursor or any future operational PROMETHEUS. For the upper stage version of those engines an expansion ratio of $\epsilon = 59$ is selected as for the SLME.

2.2. In-Air-Capturing Recovery Strategy

A returning winged first stage can be mainly recovered by two different options: autonomous flight to a landing site, the so-called LFBB (liquid fly-back booster) method, or some kind of downrange landing or recovery. The LFBB method obligates an additional propulsion system and hence fuel, which raises the stage's inert mass. The patented "In-Air-Capturing" method [10] offers a different approach with better performance: the winged stage is to be caught in the air, and towed back to the landing site without any necessity of an additional airbreathing propulsion system [11]. The idea has similarities with the downrange landing on barges that SpaceX is practicing, however, not landing on ground but "landing" in the air. Thus, additional infrastructure is required, mainly a capturing aircraft. Second-hand, refurbished and modified commercial airliners should be sufficient for the task, as was studied in [5] and [15].

A typical mission featuring IAC consists of the following phases (compare Fig. 3). First, the ascent is similar to that of a conventional ELV. After MECO the reusable winged stage is separated from the rest of the launch vehicle and travels along a ballistic trajectory, soon reaching denser atmospheric layers. Once reaching subsonic velocity the stage enters a state of equilibrium gliding flight with a constant flight path angle. At this point the reusable stage is awaited by the capturing aircraft. Both vehicles achieve formation flight in which the capturing aircraft actively matches the returning stage's velocity, heading and flight path angle. An aerodynamically controlled capturing device, which is attached to the aircraft by a rope, is achieving the close-range manoeuvring and mechanical capturing. After successful connection, the winged reusable stage is towed by the large carrier aircraft to the landing site. Close to the airfield, the stage is released, and autonomously lands on the airstrip [12], [16].

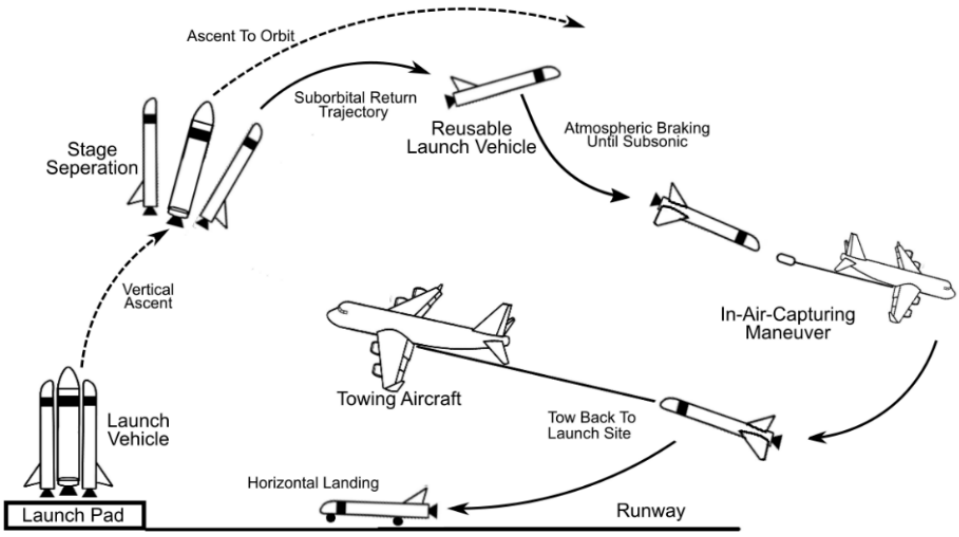

Fig. 3: Typical Mission Profile for an In-Air-Capturing mission

From a performance perspective, the IAC mode is highly attractive. Past studies on comparing different reusability methods with each other have shown, that for all investigated propellant combinations and engine cycles the RLV stages with IAC have a performance advantage not only when compared to the LFBB with turbojet flyback, but also in comparison to the DRL-mode used by SpaceX for GTO-missions [2], [3], [5]. Thus, "In-air-capturing" is an innovative and performant return method suitable for winged RLV stages.

DLR together with other partners from industry and academia is currently preparing for flight testing the "in-air-capturing"-method on a laboratory scale by using two fully autonomous test vehicles. The EC funded project FALCon should bring the TRL of the advanced IAC-recovery method beyond 4 in 2022. Preliminary results of the full-scale formation flight simulations that were conducted in FALCon are presented in [16]. After DLR had patented the IAC method for application in future RLVs, two similar approaches have been proposed. However, those named *mid-air retrieval* or *mid-air capturing* are relying on parachute or parafoil as lifting devices for the reusable parts (ULA "Vulcan"-launcher) and helicopters as capturing aircraft. Also, Rocketlab is trying to recover the Electron's first stage, returning to earth on a parachute, by catching it with a helicopter in-air.

2.3. GTO Insertion Strategy

The mission profile of the 3STO systems is shown in Fig. 4. In order to ensure that the uncontrolled descent of the expendable second stage safely occurs in the Pacific Ocean; the ascent phase is split into two steps. First, the second stage plus third stage and payload are injected into an intermediate orbit with an apogee height of 400 km to 600 km and a perigee height from 35 to 60 km. Following separation of the third stage from the second stage the third stage coasts along a ballistic trajectory. Slightly before crossing the equator the third stage is ignited to insert the payload into a GTO with 250 km or 600 km perigee and 35786 km apogee and 5.4° inclination.

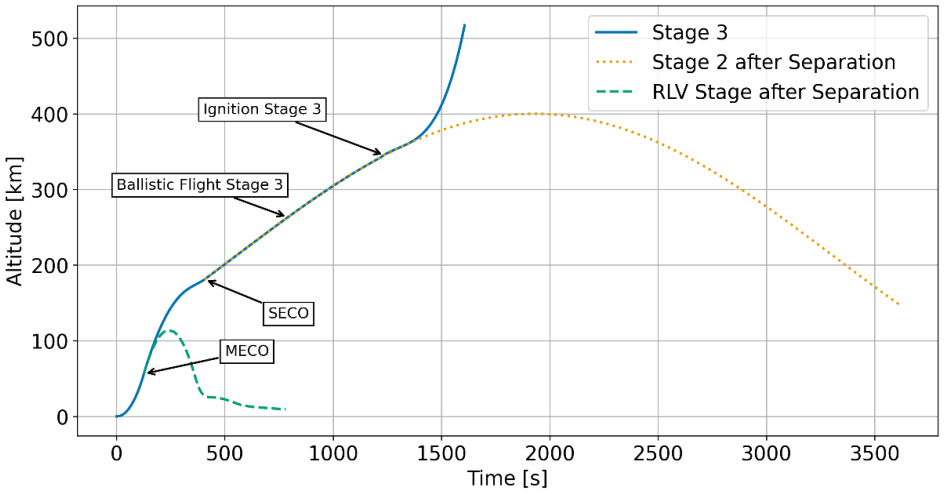

Fig. 4: Exemplary ascent and descent profiles of 3STO configurations to GTO

3. 3STO concepts

In this paper, four different 3-STO concepts are briefly described and compared. First, a version featuring the SLME engines in both RLV stage and second stage. Second, a version featuring the Prometheus hydrogen engine in those respective stages. Third, a version with Prometheus-M in the first and Prometheus-H in the second stage (hybrid) and lastly a version with Prometheus-M.

3.1. Size and Geometry

Table 3 lists the technical data of the investigated concepts. The third stage is identical for all versions, being propelled by the LOX-LH2 driven Vinci. The entire third stage is placed beneath the fairing, hence features a smaller diameter of 4 m compared to the rest of the launch stack (refer to Fig. 1). As large payloads could require more space than is available, a longer fairing or interstage should be investigated in future work. The second stage is approximately the same size for all the hydrogen versions. It is based on the current Ariane 6 core stage, hence featuring a diameter of 5.4 m for all upper stages. Because of a slightly higher propellant mass in the gas generator versions and a different engine, the Prometheus-H based stages are slightly longer. In contrast, the methane expandable second stage, although equipped with about 230 tons of propellant, ends up at 41.5 m length due to the higher density of the LOX-LCH4 propellant combination.

A general comparison of all vehicle's RLV stages as well as the Ariane 64 can be seen in Fig. 5. The RLVs have a similar size compared to the Ariane 6, but with a slightly higher payload capability of 14

tons to GTO (Ariane 64: ~11.5 tons to GTO). In general, the size of the RLV stages are relatively similar and only differ by about 10 meters in length. The main difference is the increased length of the LOX-LH2 Prometheus version due to the higher propellant loading compared to the staged combustion version. Together with the first stage of the purely methane version it features also an increased diameter of 6 m to account for the high volumetric demand.

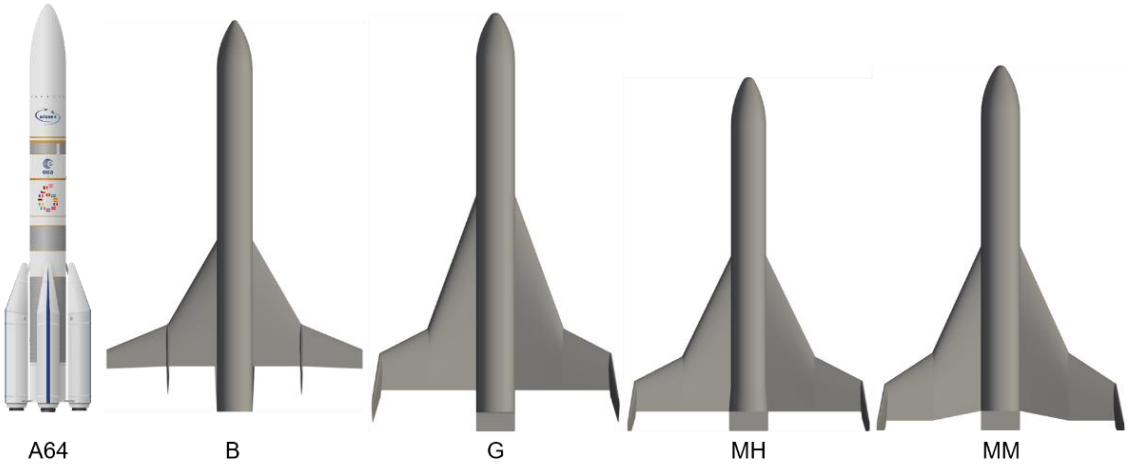

Fig. 5: Comparison of all RLV stages with the Ariane 64

Another point worth mentioning is the fact that the wing area and also wing position differs for each version. The wing area mainly depends on the stage's re-entry mass, requiring larger area for heavier vehicles. The position of the wing is determined by the position of the stage's center of gravity (CoG). Since the stage carries almost no propellant upon re-entry, the CoG position is vastly influenced by the number of engines at the rear, shifting the CoG rearwards the more engines are accommodated in the rear skirt. Thus, the position of the wing moves towards the rear for the methalox versions using a lot of engines.

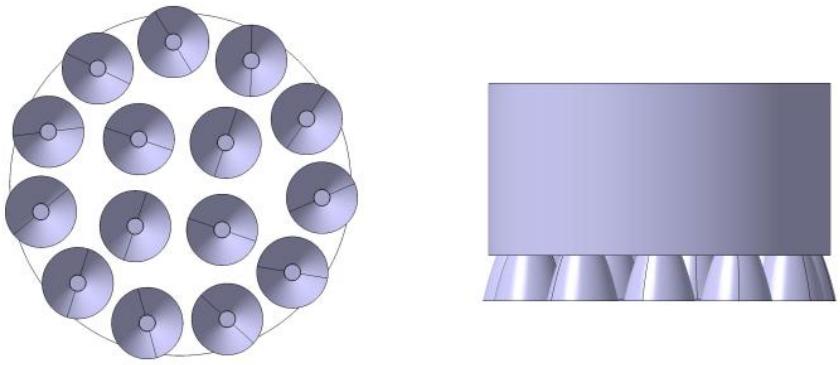

Fig. 6: Possible engine arrangement for MM first stage with 15 Prometheus-M engine

A concern with regards to the MM version is the number of engines that necessarily have to be installed in the rear skirt. Hence, a preliminary study of engine arrangement in the rear skirt was performed. A possible engine arrangement for the RLV first stage with 6 m diameter and 15 Prometheus-M engines is shown in Fig. 6. Here, the outer engines are installed without gimballing capability whereas the center engines can gimbal about 7° each independently. Whether this is sufficient can only be determined by ascent and descent 6-DOF trajectory analysis including controls in the loop, which was not performed at this early stage of design. Another consideration is the fact that the outer engines overlap the rear skirt by a small extent. This is also implemented for the SuperHeavy booster of SpaceX where the outer engines overlap the external diameter of the rocket, but it would require further aerothermal analysis to validate if this solution works. Finally, increasing the diameter of the rear skirt only towards the engine bay could allow for a more convenient arrangement, however, reducing L/D in subsonic gliding. This option will be considered in future work.

3.2. Mass

A detailed mass estimation breakdown for all versions is listed in Table 4, including margins for all elements. A more detailed breakdown is presented in [17] and [18]. The structural index (SI) shown for each stage is calculated based on the dry mass and the propellant mass (see equation (1)) and is a parameter for the overall structural efficiency.

$$\mathbf{SI} = \frac{\mathbf{m_{dry}}}{\mathbf{m_{prop}}} \tag{1}$$

Considering total lift-off mass (GLOM) the launchers get heavier the less average Isp the propellant combination has, thus leading to highest GLOM for purely methane-based launch vehicles. The lightest launcher is the LOX-LH2 version with staged combustion SLME engines with a GLOM of 665 tons. In contrast, the MM Prometheus version has a GLOM of 1203 tons, so almost double the weight. The hybrid MH version is still heavier than the gas generator LOX-LH2 version but at lower total volume and a more compact build due to the higher density of the methane-LOX combination.

Table 3: Launcher mass estimations by stage including margins

	Version SC LH_2-SC	**Version G LH_2-GG**	**Version MH Hybrid-GG**	**Version MM LCH_4-GG**
Stage 1	**H370**	**H450**	**C620**	**C800**
Dry mass	78.8 t	95.1 t	84.5 t	105.4 t
Total Propellant	378.2 t	456.8 t	628.2 t	810.2 t
GLOM	457.0 t	551.9 t	712.7 t	915.6 t
Structural index	20.8 %	20.8 %	13.5 %	13.0 %
Engines	4 x SLME	10 x Prometheus-H	11 x Prometheus-H	15 x Prometheus-M
Diameter	5.4 m	6.0 m	5.4 m	6.0 m
Length	59.1 m	64.5 m	54.5 m	56.3 m
Stage 2	**H150**	**H152**	**H152**	**C230**
Dry mass	20.6 t	19.1 t	19.1 t	19.3 t
Total Propellant	153.6 t	155.6 t	155.6 t	234.8 t
GLOM	174.2 t	174.7 t	174.7 t	254.1 t
Structural index incl. fairing	13.4 %	12.3 %	12.3 %	8.2 %
Engines	1 x SLME vacuum	1 x Prometheus-H vacuum	1 x Prometheus-H vacuum	2 x Prometheus-M vacuum
Length	46.5 m	50.8 m	50.8 m	41.5 m
Stage 3 (under fairing)	**H14**	**H14**	**H14**	**H14**
Dry mass	4.2 t	4.0 t	4.0 t	4.0 t
Total Propellant	15.7 t	15.4 t	15.4 t	15.5 t
GLOM	19.9 t	19.4 t	19.4 t	19.5 t
Structural index incl. SYLDA	26.8 %	26.0 %	26.0 %	25.8%
Vehicle				
GLOM	665.0 t	760.1 t	920.8 t	1203.2 t
Payload	13.9 t	14.1 t	14.0 t	14.0 t

The first stage's dry masses differ by about 25 tons. The LH2 SC version marks the lower end of the spectrum with about 80 tons, although with a higher structural index compared to the G version. The upper end of the spectrum is marked by the MM-version due to its large propellant loading and high

number of engines, but at lowest structural index. The rather small MH version only has a dry mass of 85 tons, an increase of 5 tons over the SC-version. This once again shows the advantage a combination of low Isp propellants in lower stages with high-Isp propellants in upper stages can lead to a decrease in launcher size. This, however, comes at the expense of having to handle two different propellant combinations and thus having to build two different engines.

The hydrolox second stages are almost equal to each other in propellant loading, the main change is in the propulsion system. The gas generator Prometheus-H engine is estimated to be more than 1 ton lighter than its staged combustion counterpart. The structural index is quite similar for all stages with about 12%-13.5%. Only the methalox second stage version differs significantly with an increase of 80 tons in propellant loading, totaling to roughly 235 tons of propellant. Nevertheless, the higher bulk density of the LOX-LCH4 decreases the stage size and the SI to a value of 8%. The third stage is almost identical for all versions, differing only marginally in propellant loading. The SI is including the SYLDA dual-payload adapter and is about 26%.

3.3. Discussion

The designed RLVs shown herein offer high payload capability to GTO while offering potential flexibility into other orbits since they could be operated as TSTO. Such a "one vehicle serves all" philosophy allows to develop only one launch vehicle to serve all kinds of target orbits, compared to multiple vehicles for a more "launcher family" type of design philosophy. It is worth mentioning that costs are the primary driver for any launch vehicle development, and according to established cost models such as Transcost the costs are expected to scale with dry mass, since the cost of propellant is negligible. This would benefit the LOX-LH2 SC version, followed by the MH hybrid version in terms of first stage dry mass. However, the MH hybrid version comes at the expense of having to develop and build two different engines (Prometheus-H and Prometheus-M). Also, as of now, it is difficult to assess the launch costs due to a lot of unknowns and uncertainties in cost estimation, especially with regards to RLVs.

In the framework of current developments in Europe, it is important to point out the performance advantage that LOX-LH2 offers, especially when combined with a staged combustion cycle. The methalox combination is not beneficial for reusable launch vehicles, since the lower Isp requires significantly more propellant loading. The herein shown vehicles could be envisioned as a potential RLV for Europe, relying in parts on Ariane 6 heritage and Prometheus engines. With a payload capability of 14 tons to GTO they are more powerful than the Ariane 6 while offering first stage reusability by an innovative and performant return method.

4. Re-entry Aerodynamics & Flight Dynamics

Designing an aerodynamically controlled vehicle re-entering the atmosphere at hypersonic velocity, subsequently slowing down to subsonic velocity and finally reaching equilibrium gliding flight conditions, is a very challenging task. The stage covers a vast range of flight conditions at which it has to be controllable to allow a safe re-entry while also fulfilling the gliding flight requirement necessary for a successful In-Air-Capturing maneuver. Hence, understanding the flight dynamics behind the re-entry of a winged vehicle in an early design stage is necessary to identify challenges with regards to controlling and actively steering such a high-performance vehicle in order to arrive at a feasible and robust design that does not fail to converge in later design iterations.

Therefore, the LOX-LH2 SC first stage was selected as baseline concept to be subjected to a thorough analysis of re-entry aerodynamics and its effect on flight dynamics. This includes studying the impact of different design changes to the aerodynamic performance, investigating the dynamic motion and stability of the stage and, finally, studying control possibilities and simulating 6-DOF flight maneuvers.

4.1. Re-entry Trajectory

The re-entry trajectory of the RLV stage baseline with 3 degrees of freedom is shown in Fig. 7. Following MECO, the stage coasts along a ballistic trajectory until it reaches the denser parts of the atmosphere. The AoA is kept high to produce a high amount of drag and sufficient lift to keep the stage at low-density regions of the atmosphere as long as possible in order to limit the heat flux during re-entry. The heat flux is calculated according to a simplified Fay-Riddell equation with respect to a nose radius of 1 m. Hence, the heat flux shown in the figure does not represent the maximum heat flux that is expected at parts with a small leading-edge radius, like the wing and fins leading edges.

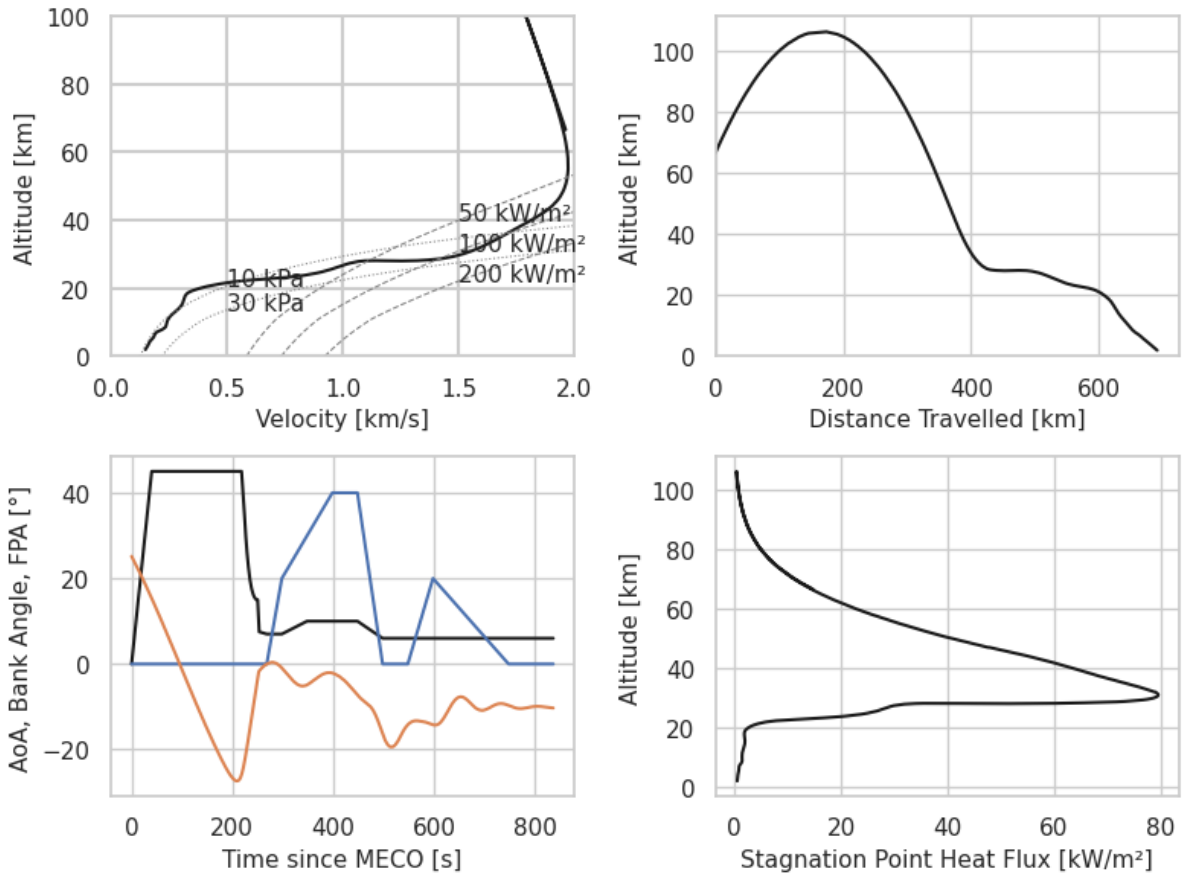

Fig. 7: Re-entry Trajectory of the LOX-LH2 SC first stage

Additionally, the vehicle flies several bank maneuvers in order to change the heading so that the stage flies towards the direction it is coming from when reaching subsonic speeds. Also, the bank angle is used to control the vertical amount of lift force produced. It is clearly visible in the trajectory control profile that a velocity-range from subsonic (Mach = 0.4) to supersonic (Mach = 7 and more) has to be covered while controlling AoAs from 0° to 40°. This requirement is rather demanding since the aerodynamic properties of the vehicle change significantly from supersonic to subsonic velocity

4.2. Aerodynamic Performance & Static Stability

One of the key parameters to evaluate the stage's aerodynamic performance is Lift-to-Drag ratio (L/D). This is depicted in Fig. 8 for the reference stage for trimmed conditions, calculated using empirical DATCOM-based estimation methods. As longitudinal trimming device, the trailing edge flaps shown in Fig. 1 are used. The L/D at supersonic flight is around 2, which is typical for such re-entry vehicles, and roughly 6.5 for subsonic flight. This high L/D value should allow to achieve quite shallow gliding flight path angles that are suitable for In-Air-Capturing.

One of the most demanding design challenges is to ensure the vehicle is longitudinally trimmable at very high AoA during re-entry and medium to low AoA later on at subsonic velocity. The right-hand plot in Fig. 8 shows the moment coefficients for different flap deflection angles for the reference stage. The wing design allows to trim high AoAs at supersonic velocity and low AoA allowing for flight at maximum L/D at subsonic velocity, thus fulfilling this requirement.

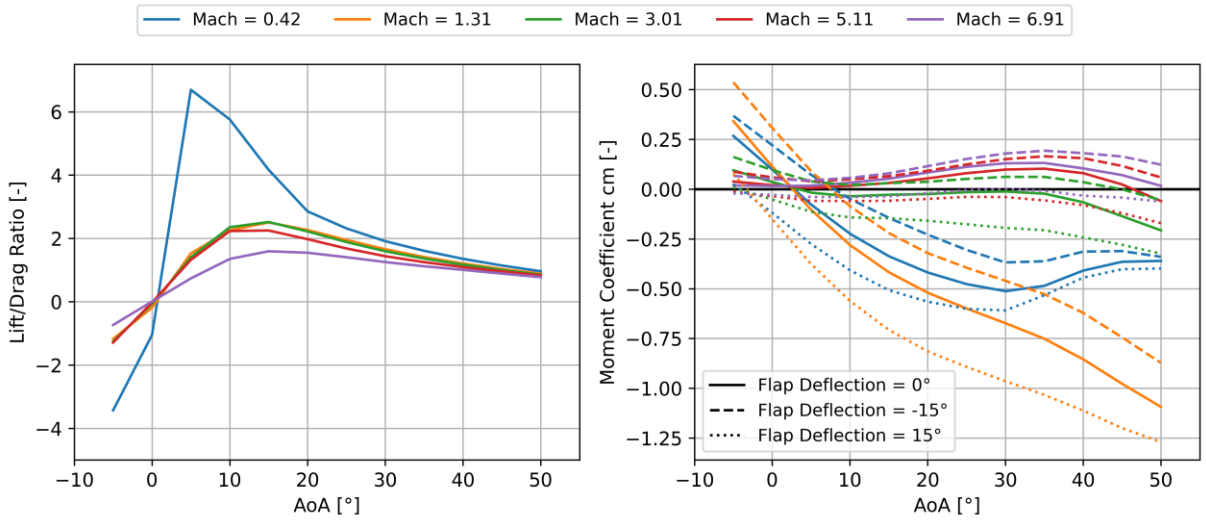

Fig. 8: Lift-to-Drag Ratio of the trimmed RLV stage at different Mach numbers

To evaluate the static stability in longitudinal and lateral direction, the common criteria for longitudinal stability (equation (2)) and directional stability (equation (3)) can be used. Here, Δcm is the derivative of pitching moment coefficient, α is the AoA, cn is the yawing moment coefficient and β is the sideslip angle.

$$\frac{\Delta cm}{\Delta \alpha} \leq 0 \tag{2}$$

$$\frac{\Delta cn}{\Delta \beta} \geq 0 \tag{3}$$

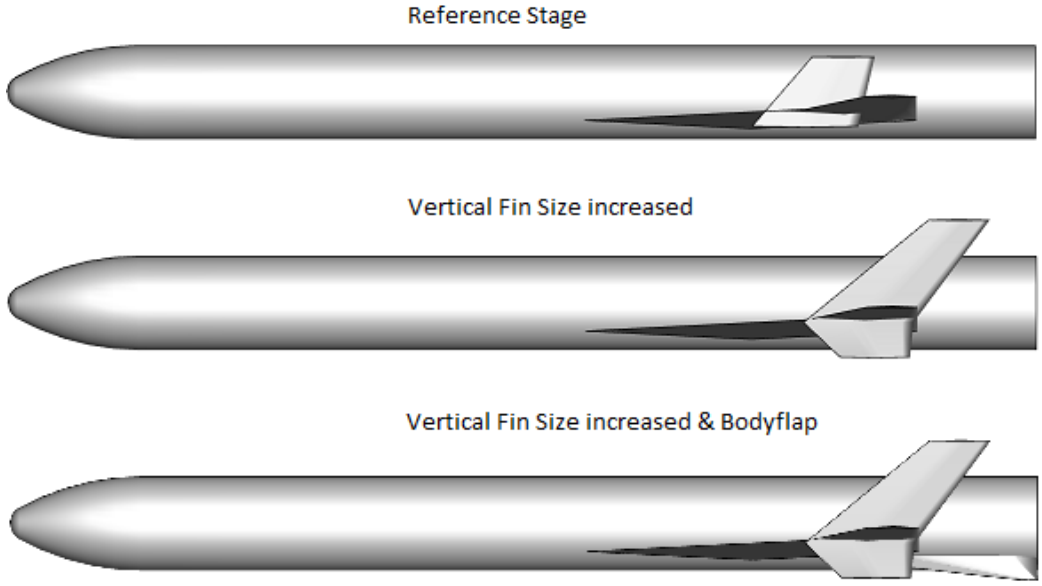

Fig. 9: RLV stage designs considered for stability analysis

For the stability analysis two variations from the reference stage were also considered (compare Fig. 9). First, a version with increased vertical fin size was considered to potentially increase lateral stability. Second, this version with increased vertical fin area was further equipped with a bodyflap which acts as part of the fuselage that can be deflected downwards (compare Fig. 9, bottom). This allows to trim high AoA at supersonic velocities better. Furthermore, the side extensions of the downward deflected bodyflap can increase directional stability.

Fig. 10 shows the pitching moment stability coefficient and Fig. 11 the respective directional stability coefficient for the three different versions over the potential Mach-AoA range. The reference trajectory is plotted in black to show the different phases the vehicle would encounter. From Fig. 10 it is clearly visible that the most of the trajectory takes place at flight conditions where the vehicle is passively, statically stable. Only at around Mach 5 the vehicle crosses a region of instability in the pitching axis. This occurs around the phase of maximum dynamic pressure, where the AoA is gradually being decreased. Also, the version with the big bodyflap and big vertical fins offers the best behavior considering pitching moment stability.

Considering lateral, or directional, stability the results are not as promising. The reference concept with the small vertical fins is statically unstable throughout all flight conditions. The two versions with greater fin size show better stability behavior at subsonic velocity, but the vehicle remains unstable throughout most parts of supersonic flight. Again, the version with increased fins and the big bodyflap renders the best results in terms of stability.

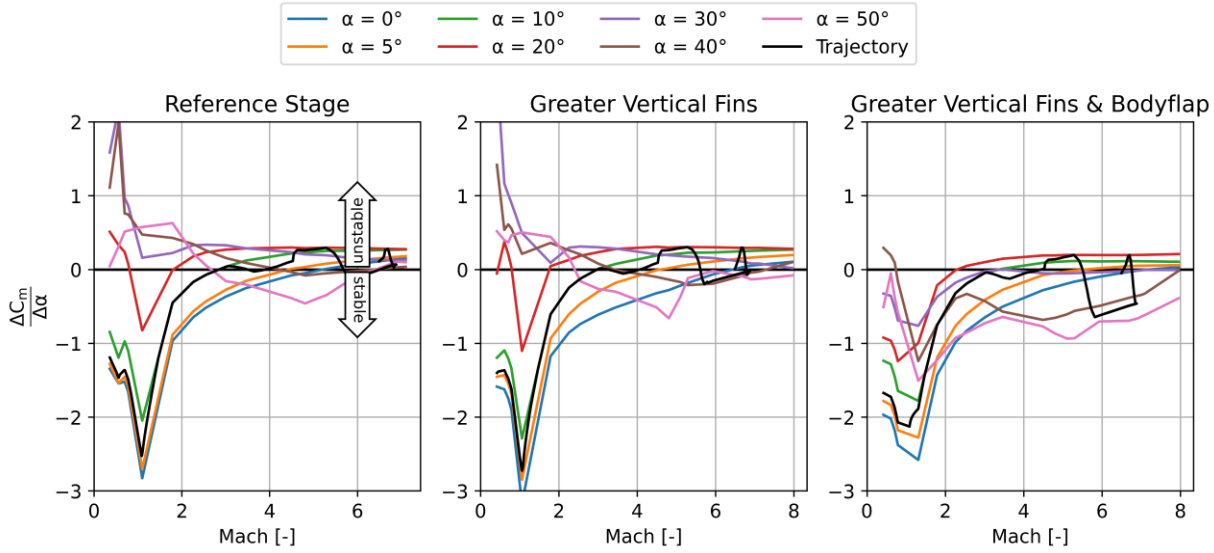

Fig. 10: Change of Pitch Moment Coefficient with respect to AoA for different AoAs and along the trajectory

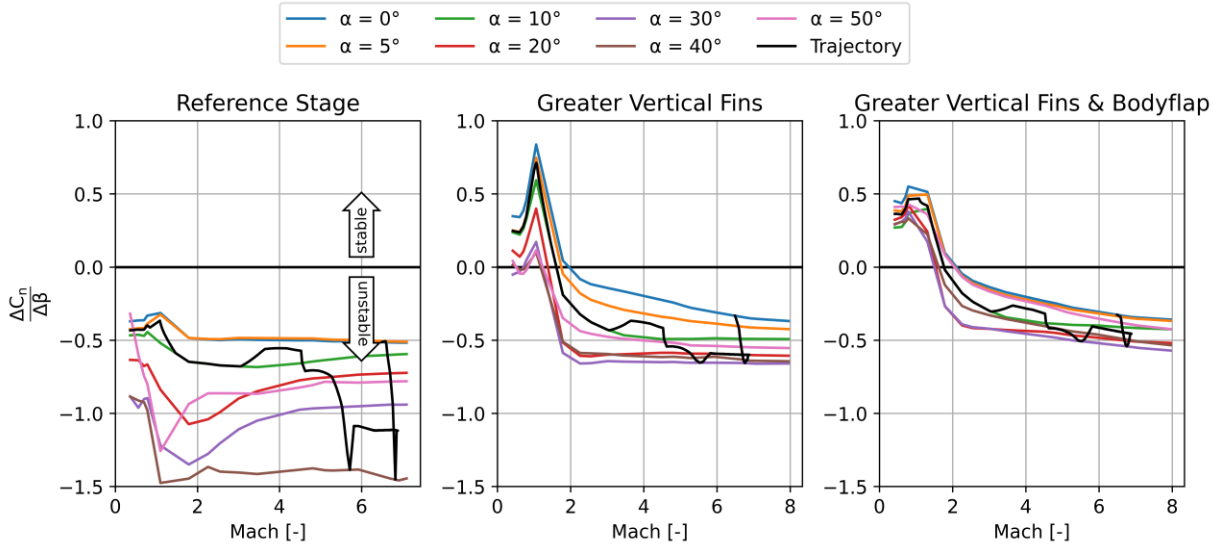

Fig. 11: Change of Yaw Moment Coefficient with respect to sideslip for different AoAs and along the trajectory

One of the reasons for the instability is the position and size of the vertical fins, which are smaller and positioned more to the front compared to the vertical fins of commercial aircraft. Furthermore, the

stage's CoG is quite aft, thus decreasing the lever-arm of the potentially stabilizing moment by the vertical fins. This, in combination with the different flow field at supersonic flight, with lower density on the upper side of the wing, leads to the instability observed. Another factor that contributes to lateral instability at high AoA is the shadowing effect of the wing onto the upper part of the fins. The DATCOM method used for aerodynamic coefficient calculation includes some kind of body-fin interaction, but the shadowing effect is most likely underestimated. Detailed insight would require CFD simulations or wind tunnel experiments.

This preliminary analysis shows that further focus has to be put onto the problem of directional instability throughout supersonic flight. Hence, the best performing design, the stage with the big vertical fins and bodyflap, will be subjected to a more detailed analysis considering also dynamic stability and control possibilities in the next section.

4.3. Re-entry Dynamics

For a complete description of the flight dynamics of the selected RLV stage (big bodyflap and big vertical fins) along a reference trajectory, the equations of motion with 6 degrees of freedom (6-DOF) are required. Those equations are non-linear and complex, hence a full 6-DOF simulation requires computational effort. A simplified and faster approach to determining flight dynamics at certain flight points is the linearization of the equations of motion. This method allows to derive linear, time-invariant equations that are valid in a range of small disturbances around an equilibrium point of the vehicle (usually trim points) and are suitable for describing the flight dynamics in this area. In addition, such linearized systems can already be used to design control loops for controlling the vehicle. Furthermore, the eigenvalues and -motions of the system at each trajectory point can be determined. The detailed procedure is described in [19].

Dynamic open-loop stability without controls actively counteracting disturbances is given if the real part of all eigenvalues is smaller than zero, hence $Re(\lambda i) < 0$. By checking the real and complex parts of the eigenvalues at specific points in the trajectory one can determine if the vehicle is stable or unstable throughout the flight regime. Fig. 12 shows the real and complex parts of the eigenvalues along the trajectory in a pole-zero plot. Eigenvalues without a complex part represent non-oscillatory movements, meaning that the respective motion is either exponentially stable or instable. Complex conjugate eigenvalues, so pairs of eigenvalues, represent oscillatory motions.

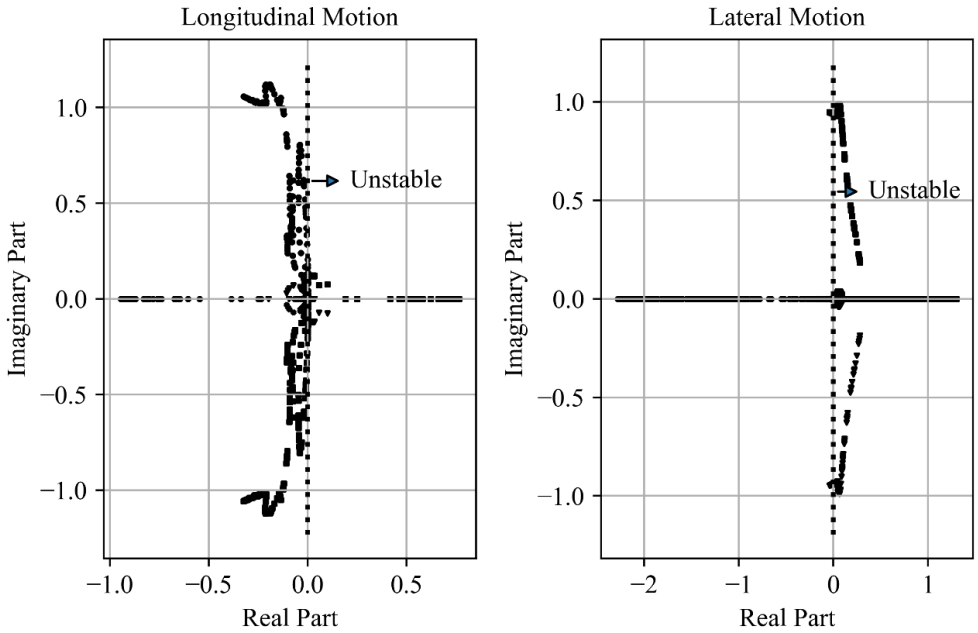

Fig. 12: Pole-Zero Plot of eigenvalues of longitudinal and lateral motion throughout the re-entry trajectory of the RLV stage

It is visible that the longitudinal motion is mostly stable throughout the trajectory. Only a few eigenvalues have a real part which is in the region of Mach 5 to Mach 3 at high to medium AoA, in accordance with the analysis shown in Fig. 10 and Fig. 11. This corresponds to the region of maximum

dynamic pressure during re-entry where a different AoA cannot be easily achieved. Hence, active control at this point is crucial to keep the commanded AoA profile. Contrary to that, the lateral motion is unstable throughout most of the flight. In fact, even down to Mach 0.5 there is at least almost always one unstable eigenvalue. This observance supports the point that was already concluded by the analysis by stability derivatives, namely that the lateral motion is the more critical motion in terms of stability.

The eigenvalues can further be used to derive the frequency, damping, period T and time to half amplitude t_{HA} [19]. This is exemplary shown for two different flight points, one at subsonic velocity (Mach = 0.44) and one for high velocity (Mach = 5.63) with high AoA during the initial phase of re-entry in Table 4 for the critical lateral movement. At subsonic velocity, we can observe common motion responses such as a highly damped roll movement, called the roll mode, a medium damped motion called spiral mode and a classical "dutch roll", defined as a constant, mostly low-damped oscillation in sideslip and roll.

Table 4: Eigenvalues, period T and time to half amplitude t_{HA} for the lateral motion at different flight conditions

Mach	AoA	Altitude	T	t_{HA}	Mode
0.44	12.0°	8.1 km	-	0.3 s	Roll Mode
			-	30.8 s	Spiral Mode
			6.6 s	22.1 s	Dutch Roll
5.63	35°	38.5 km	-	0.7 s	Stable Mode 1
			-	5.5 s	Stable Mode 2
			-	-0.8 s	Unstable Mode 1
			-	-40 s	Unstable Mode 2

Nevertheless, at supersonic velocity, the picture switches and different kind of motions are observed. Now there are only exponential modes of which two are unstable and the other two represent stable motions. The time-to-half-amplitude in the worst case is -0.8 s, the negative sign indicating that the amplitude actually increases. This motion mainly occurs around the vehicles vertical axis (sideslip) and any disturbance is doubled within 0.8 s in this motional mode. Here, active and fast control is crucial and shall be investigated in the following section.

4.4. 6-DOF Simulation

The analysis of dynamic stability in the previous section has shown the need for an active and fast control in order to stabilize the vehicle throughout re-entry. Therefore, an active control loop is assumed with full state feedback and infinitely fast actuators. This is a simplification which was deemed suitable at this early design state of the vehicle. Including actuator and sensor models could be focus of future work. Furthermore, no wind or atmospheric disturbance was assumed yet.

The control design is based on the work presented in [19] and features using linear quadratic regulator methods (LQR) at certain flight points to obtain the feedback gains which are then manually tuned to achieve the desired control behavior. For pitch control, the inner trailing edge flaps as shown in Fig. 1 are used, for roll control the outer flaps are used and for yaw control, the vertical fins can be deflected entirely. Additionally, an RCS is required for exo-atmospheric control, which is positioned in the nose of the stage. For each axis, 4 RCS engines are foreseen, with a vacuum Isp of 250 s and a thrust of 650 N each. The distance to the CoG is estimated at 30 m along the x-axis. The minimum impulse duration of one RCS pulse is set to t = 0.05 s.

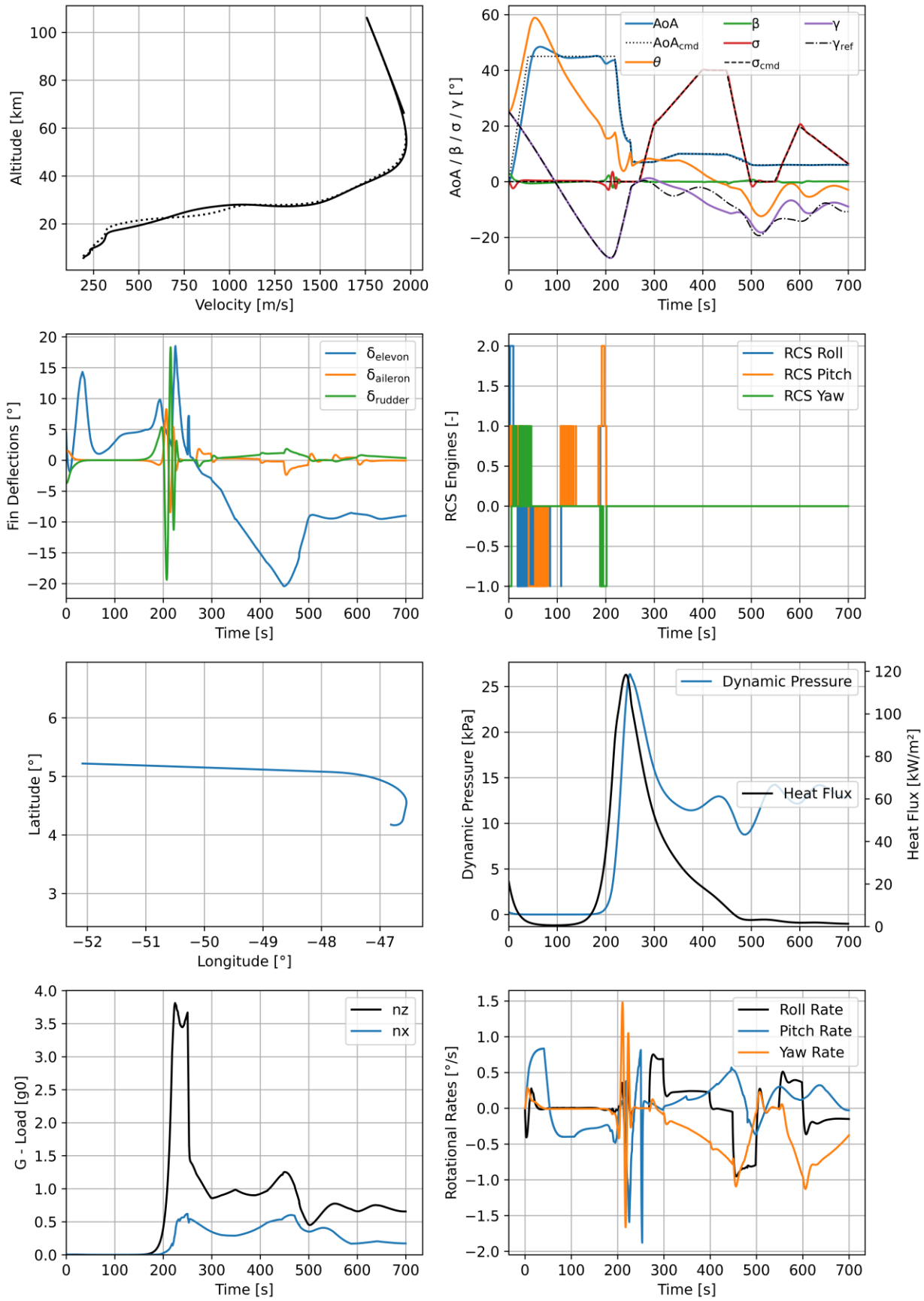

Fig. 13: 6-DOF simulated re-entry of reference RLV stage with control in the loop

Using the reference trajectory shown in Fig. 7, the AoA and bank angle profile from this trajectory are used as actively commanded controls for the trajectory. The 6-DOF simulation is initiated at MECO conditions with a disturbance of 0.05 rad in sideslip in order to simulate an angular offset from the optimum and to demonstrate the vehicle's capability to counteract disturbances. The 6-DOF simulated trajectory is shown in Fig. 13. The initial phase with RCS is clearly visible with the engines activating according to the control needs. After around 200 s into return flight, the RCS is deactivated when reaching a dynamic pressure threshold of 1 kPa. Here, the aerodynamic control surfaces take over completely, with their control authority calculated by using a blending function that is dependent on the dynamic pressure.

This initial part of the re-entry is highly critical, as can be seen by the oscillations arising in this part. The vehicle transitions from RCS to aerodynamic control at a flight condition where it is naturally unstable (high AoA, high velocity). As there is a slight deviation in sideslip and roll angle, due to the limit-cycle control by the RCS, the aerodynamic surfaces start oscillating in order to stabilize the vehicle. Here, more off-nominal conditions could render the vehicle unstable and lead to loss of control. However, this could be counteracted by better controller tuning, which could be solved in future work.

Once trespassing the critical phase, the vehicle is capable of following the commanded AoA and bank angle profile with very good accordance. The point of maximum dynamic pressure is a flight condition of high sensitivity for the vehicle, so extra care has to be taken to adequately tune the controllers in order to find a robust solution here. At subsonic velocity, the flight path angle can be kept around -10° with a velocity of 200 – 240 m/s, depending on the altitude, which should allow for good conditions for the In-Air-Capturing maneuver.

For future work, a further control loop taking the desired heading, altitude and velocity as commands could be envisioned in order to stay closer to the reference trajectory. The deviations between 6-DOF and 3-DOF trajectory in Fig. 13 mainly come from the imperfections in following the commanded control profile and deviating aerodynamic coefficients due to the fin and flap deflections contributions being included. Nevertheless, the goal of demonstrating that re-entry of such a passively stable vehicle with active controls is possible was proven. Future work will focus on elaborating on aspects such as fastness of actuators, a realistic feedback of sensor data on the state and potentially, including atmospheric disturbances like wind.

5. Conclusion

In this paper, the design of various winged reusable launchers for a future European system has been investigated. With three stages, these are high performance launchers exceeding the current payload target of the Ariane 6. The resulting designs show clear differences depending on the choice of propellant combination and engine cycle. From a mass perspective, the hydrolox version with the full-flow staged combustion engine SLME has clear advantages because it offers the lowest GLOM and structural mass. However, there is currently no major development effort with regards to developing a full-flow staged combustion hydrolox engine in Europe.

The advantage of the methane versions is that a modern European engine demonstrator with this fuel is already in development with Prometheus. However, with both first stages featuring methalox engines, this results in a large and heavy launcher with up to 15 engines in the first stage and 2 in the second stage. Due to its mass, this also creates challenges during re-entry as well as capturing and tow-back. Both from an overall design as well as a mass perspective, the version MH combines the advantages of a small RLV stage with the efficiency of the hydrogen second stage making it an attractive option. However, on the negative side it would require operation and handling of two different propellants as well as not being able to fly "used" RLV engines for a final mission on the upper stage.

Also, a selected RLV reference stage was investigated in detail with regards to return trajectory, aerodynamics and flight dynamics during re-entry. As it turns out the RLV stages are potentially instable in lateral movement, especially with regards to the so-called directional, or weathercock, stability. Here, either design improvements, such as bigger vertical fins or active control are necessary to stabilize the stage. A preliminary, simplified 6-DOF analysis using RCS and aerodynamic control surfaces to steer the vehicle, shows that the reference profile in AoA and bank angle can be followed. However, a more detailed model including wind, actuator models and sensor models would increase the insight and should be in focus of future work.

For future studies, these launcher system designs need to be expanded and must be investigated in more detail. Furthermore, the design of the wing and its capabilities for re-entry and in-air-capturing must be a focus in the future beyond the predevelopment analysis performed here. All in all, the systems analyzed provide a good starting point for the discussion about the next generation European launchers including a new innovative recoverability method.

Acknowledgements

Part of this work was performed within the project '**F**ormation flight for in-**A**ir **L**auncher 1st stage **C**apturing dem**on**stration' (**FALCon**) addressing development and testing of the "in-air-capturing" technology. FALCon, coordinated by DLR-SART, is supported by the EU within the Horizon2020 Programme 5.iii*. Leadership in Enabling and Industrial Technologies – Space* with EC grant 821953. Further information on FALCon can be found at http://www.FALCon-iac.eu

References

[1] Patureau de Mirand, A.; Bahu, J.M.; Louaas, E.: Ariane Next, a vision for a reusable cost efficient European rocket, 8TH EUROPEAN CONFERENCE FOR AERONAUTICS AND SPACE SCIENCES (EUCASS), Madrid 2019

[2] J. Wilken, S. Stappert, L. Bussler, M. Sippel, E. Dumont, *Future European Reusable Booster Stages: Evaluation of VTHL and VTVL Return Methods*, 69th IAC, Bremen, Germany, 1st -5th October 2018

[3] S. Stappert, J. Wilken, L. Bussler, M. Sippel, *A Systematic Comparison of Reusable First Stage Return Options*, 8th European Conference for Aeronautics and Space Sciences, Madrid, Spain, 1st – 4th July 2019

[4] M. Sippel et al., *Focused Research on RLV technologies: the DLR project AKIRA*, 8th European Conference for Aeronautics and Space Sciences, Madrid, Spain, 1st – 4th July 2019

[5] M.Sippel et al., *Highly Efficient RLV-Return Mode "In-Air-Capturing" Progressing by Preparation of Subscale Flight Tests*, 8th European Conference for Aeronautics and Space Sciences, Madrid, Spain, 1st – 4th July 2019

[6] Sippel, M., Stappert, S., Bussler, L., Callsen, S.: *High-Performance, Partially Reusable Launchers for Europe,* Proceedings of the International Astronautical Congress, IAC. 71st International Astronautical Congress (IAC 2020), 12.-14.10.2020, Cyberspace Edition. ISSN 0074-1795.

[7] M. Sippel, J. Wilken, Preliminary Component Definition of Reusable Staged-Combustion Rocket Engine, Space Propulsion 2018, Seville, Spain, May 2018

[8] M.Sippel, S. Stappert, C. Messe, L. Bussler, *Powerful & Flexible Future Launchers in 2- or 3- stage configuration,* 70th IAC, Washington DC, USA, 21st – 25th October 2019, IAC-19-D2.4.8

[9] M. Sippel, J. Wilken: *Preliminary Component Definition of Reusable Staged-Combustion Rocket Engine*, Space Propulsion 2018, Seville, May 2018

[10]Patentschrift (patent specification) DE 101 47 144 C1, *Verfahren zum Bergen einer Stufe eines mehrstufigen Raumtransportsystems*, released 2003

[11] Sippel, M.; Klevanski, J.; Kauffmann, J.: *Innovative Method for Return to the Launch Site of Reusable Winged Stages*, IAF-01-V.3.08, 2001

[12] Sippel, M., Klevanski, J.: *Progresses in Simulating the Advanced In-Air-Capturing Method*, 5th International Conference on Launcher Technology, Missions, Control and Avionics, S15.2, Madrid, November 2003

[13] Sippel, M., Stappert, S., Pastrikakis, V., Barannik, V., Maksiuta, D., Moroz, L.: *Systematic Studies on Reusable Staged-Combustion Rocket Engine SLME for European Applications*, 8th Space Propulsion Conference 2022, 09.-13.05.2022, Estoril, Portugal.

[14] Simontacchi, P., Edeline, E., Blasi, E. et al.: PROMETHEUS: PRECURSOR OF NEW LOW-COST ROCKET ENGINE FAMILY, 69th International Astronautical Congress (IAC), Bremen, Germany, 2018

[15] Stappert, S., Wilken, J., Dominguez G. J. C., Sippel, M.: *Evaluation of Parametric Cost Estimation in the Preliminary Design Phase of Reusable Launch Vehicles*, 9th Conference on Aeronautics and Space Sciences (EUCASS), 2022. 9th European Conference on Aeronautics on Space Sciences (EUCASS), 27.06.-01.07.2022, Lille, France

[16] Singh, S., Bussler, L., Stappert, S., Sippel, M., Kucukosman, Y. C., Buckingham, S.: *Simulation and Analysis of Pull-Up Manoeuvre during In-Air Capturing of a Reusable Launch Vehicle*, 9th European Conference for Aeronautics and Space Sciences (EUCASS), 27.06- 01.07 2022, Lille, France.

[17] Callsen, S., Stappert, S., Sippel, M.: *Study on future European winged reusable launchers,* 9th European Conference For Aeronautics And Space Science, EUCASS 2022. 9th European Conference for Aeronautics and Space Sciences (EUCASS), 27.06 - 01.07 2022, Lille, France

[18] Sippel, Martin et al.: *A viable and sustainable European path into space – for cargo and astronauts*, Proceedings of the International Astronautical Congress, IAC. 72nd International Astronautical Congress (IAC), 25.-29.10.2021, Dubai. ISSN 0074-1795

[19] Stappert, Sven und Callsen, Steffen und Sippel, Martin: *Re-entry and Flight Dynamics of a Winged Reusable First Stage,* 9th European Conference on Aeronautics and Space Sciences (EUCASS), 2022. 9th European Conference for Aeronautics and Space Sciences (EUCASS), 27.6.-01.07.2022, Lille, France